# A Century Of Reforestation Reduced Anthropogenic Warming in the Eastern United States

**Mallory L. Barnes[1]*, Quan Zhang[2], Scott M. Robeson[3], Lily Young[1], Elizabeth A. Burakowski[4], A. Christopher. Oishi[5], Paul C. Stoy[6], Gaby Katul[7], Kimberly A. Novick[1]***

[1] O'Neill School of Public and Environmental Affairs, Indiana University, Bloomington, IN, United States
[2] State Key Laboratory of Water Resources and Hydropower Engineering Science, Wuhan University, Wuhan, China
[3] Department of Geography, Indiana University, Bloomington, IN, United States
[4] Institute for the Study of Earth, Oceans, and Space, University of New Hampshire, Durham, NH, United States
[5] USDA Forest Service, Southern Research Station, Coweeta Hydrologic Laboratory, Otto, NC, United States
[6] Department of Biological Systems Engineering, University of Wisconsin–Madison, United States
[7] Department of Civil and Environmental Engineering, Duke University, Durham, NC, United States

Corresponding author: Mallory Barnes (malbarn@iu.edu)

* Mallory Barnes & Kim Novick are both corresponding authors (malbarn@iu.edu; knovick@iu.edu)

**Key Points:**

- Reforestation in the eastern United States (EUS) contributes to cooling the land surface and near-surface air temperature.
- The biophysical impacts of reforestation help explain the anomalous lack of 20$^{th}$-century warming in the EUS
- Reforestation in temperate regions has the potential to provide biophysical climate adaptation benefits by cooling surface and air temperatures.

## Abstract

Restoring and preventing losses of the world's forests are promising natural pathways to mitigate climate change. In addition to regulating atmospheric carbon dioxide concentrations, forests modify surface and near-surface air temperatures through biophysical processes. In the eastern United States (EUS), widespread reforestation during the 20th century coincided with an anomalous lack of warming, raising the question of whether reforestation contributed to biophysical cooling and slowed local climate change. Using new cross-scale approaches and multiple independent sources of data, our analysis uncovered links between reforestation and the response of both surface and air temperature in the EUS. Ground- and satellite-based observations showed that EUS forests cool the land surface by 1-2 °C annually, with the strongest cooling effect during midday in the growing season, when cooling is 2 to 5 °C. Young forests aged 25-50 years have the strongest cooling effect on surface temperature, which extends to the near-surface air, with forests reducing midday air temperature by up to 1 °C. Our analyses of historical land cover and air temperature trends showed that the cooling benefits of reforestation extend across the landscape. Locations predominantly surrounded by reforestation were up to 1 °C cooler than neighboring locations that did not undergo land cover change, and areas dominated by regrowing forests were associated with cooling temperature trends in much of the EUS. Our work indicates that reforestation contributed to the historically slow pace of warming in the EUS, highlighting the potential for reforestation to provide local climate adaptation benefits in temperate regions worldwide.



## Plain Language Summary

A century of eastern US reforestation has had a cooling effect that helps to explain a lack of regional warming in the 20th century, which stands in contrast to warming trends across the rest of North America during the same period. Our study shows that forests across much of the eastern United States have a substantial adaptive cooling benefit for surface temperature, and for the first time, we demonstrate that this benefit also extends to near-surface air temperature. Therefore, reforestation in temperate zones could provide a complementary set of benefits: mitigating climate change by removing carbon dioxide from the atmosphere, while also helping us adapt to rising temperatures by cooling surface and air temperatures over large areas.


## 1 Introduction

Drastic reductions in anthropogenic greenhouse gas emissions are necessary to address climate change. Nature-based Climate Solutions (NbCS), such as reforestation, have the potential to provide additional mitigation through atmospheric $CO_2$ removal (Nolan et al., 2021; Novick et al., 2022a,b; Seddon et al., 2020), but will only be effective if they are accompanied by economy-wide decarbonization. Changes to land cover and management, which are central to the implementation of NbCS, can alter local temperature through changes to the surface energy balance (Anderson et al., 2011). If these biophysical impacts are beneficial, then some NbCS could serve as a tool for local adaptation in addition to global-scale climate mitigation.

Reforestation – the NbCS with the highest $CO_2$ mitigation potential (Griscom et al., 2017) – can increase or decrease local surface temperature ($T_s$) depending on the balance of competing mechanisms. In the tropics, forests evaporate substantially more water than grasslands, which promotes cooling by using energy that would otherwise heat the surface (Anderson et al., 2011;

Williams et al., 2021). Conversely, reforestation in boreal climates tends to warm the surface through reductions in albedo (Lee et al., 2011). In the temperate zone, surface cooling from increased evaporative and sensible heat fluxes usually outweighs albedo-driven warming, such that temperate forests have lower $T_s$ compared to non-forested ecosystems (Anderson et al., 2011; Bright et al., 2017; Windisch et al., 2021; Zhang et al., 2020).

Although $T_s$ is relevant to many ecological processes (Farella et al., 2022), the near-surface air temperature ($T_a$) is an equally important target for climate adaptation (Novick & Katul, 2020; Winckler et al., 2019) because changes in $T_a$ can have far-reaching effects, as biophysical impacts on air temperature can be advected across the landscape (Winckler et al., 2019). While land-cover change affects $T_s$ and $T_a$ differently (Baldocchi & Ma, 2013; Helbig et al., 2021; Novick & Katul, 2020; Winckler et al., 2019), quantifying the impacts of land-cover change on $T_a$ has historically been challenging. Near-surface air temperature cannot be sensed remotely, and its variation with height makes it hard to measure and interpret over forests (Novick & Katul, 2020; Winckler et al., 2019). Most data-driven studies investigating biophysical impacts on both $T_s$ and $T_a$ typically compare locations with similar macroclimates but different land cover, which captures the direct, local effects of land-cover change on $T_s$ and $T_a$ (e.g., Baldocchi & Ma, 2013; Bright et al., 2017; Juang et al. 2007; Winckler et al., 2019; Windisch et al., 2021; Zhang et al., 2020). However, this approach can overlook indirect, non-local effects (Baldocchi & Ma, 2013) related to advection or changes in downstream cloud cover due to increased upstream evapotranspiration. This study adopts a novel combination of approaches to evaluate the impacts of reforestation on both $T_s$ and $T_a$, exploring both local and larger-scale effects across various spatial and temporal scales.

The Eastern United States (EUS) has undergone extensive reforestation over the last century (Figs. 1A, B; Meehl et al., 2012), providing a unique opportunity to investigate the biophysical impacts of large-scale land cover change. Additionally, the absence of warming over a large portion of the EUS during this period (Fig. 1C; Ramankutty et al., 2010) raises the question of whether reforestation has dampened the historic pace of warming in the region. To address this question, we employ multiple independent data sources to evaluate both local and non-local effects of reforestation on $T_s$ and $T_a$. Our approach involves: 1) comparing locations with similar climates but different land cover using both satellite and *in situ* observations to determine the local effects of reforestation on $T_s$ and $T_a$, 2) exploring gradients in $T_s$ across ecosystem boundaries to uncover the potential local extent of such effects, and 3) analyzing historical weather station, air temperature, and land-cover data to identify long-term links between $T_a$ and forest cover trends at landscape and regional scales. Through this comprehensive approach, we aim to gain insight into the extent to which EUS reforestation has influenced historical rates of regional warming and the potential of temperate zone reforestation for climate adaptation.

**1.1 Historic land cover and climate trends in the region.** Before European settlement, forests occupied most of the land area in the EUS, with an uneven-aged stand structure sustained by selective harvest and controlled burning by Indigenous tribes (Meehl et al., 2012). However, from the late 18$^{th}$ to early 20$^{th}$ century, forest cover in the EUS dramatically decreased due to harvesting for timber and clearing for agriculture, resulting in forest losses exceeding 90% in some locations (Carman, 2013; Hall et al., 2002; Houghton & Hackler, 2000). By 1930, widespread land clearing had largely stopped, and forest cover began to increase with the abandonment of marginal agricultural fields and active reforestation efforts (Carman, 2013; Hall

et al., 2002; Houghton & Hackler, 2000; Meehl et al., 2012). Since 1900, millions of hectares of forest have been added in the northeastern, southeastern, and midwestern US (Fig. 1B, and Carman, 2013; Hall et al., 2002; Wear & Greis, 2012), mostly through the conversion of crop and pastureland to deciduous forests, or to pine plantations providing softwood timber in some parts of the southeastern US (Mascioli et al., 2017). Many forests in the region are now 50-100 years old (Fig. 1C, Fig. S1), although frequent harvest of pine plantations suppresses stand age in the Southeast.

This century of EUS reforestation coincides with an anomalous lack of regional warming, sometimes referred to as a 'warming hole' (Fig. 1; Mascioli et al., 2017; Meehl et al., 2012; Z. Pan et al., 2004; Partridge et al., 2018; Tosca et al., 2017). While most land areas worldwide warmed during the twentieth century, much of the EUS experienced minor cooling, from -0.2 ° C to -0.8 °C per 50 years (Fig. 1C). Proposed explanations for this cooling include internal climate variability (Mascioli et al., 2017; Meehl et al., 2012), anthropogenic aerosols (Tosca et al., 2017), agricultural intensification (Mueller et al., 2016), and increasing precipitation (Z. Pan et al., 2004). However, mechanistic attribution remains elusive (Mascioli et al., 2017; Partridge et al., 2018), and some of the mechanisms (e.g., agricultural intensification) are not relevant across the entire extent of the warming hole. Despite the established potential of reforestation to affect local temperature, the biophysical impacts of regional reforestation over the past century have not been thoroughly evaluated for their contribution to the 'warming hole' in the EUS.

## 2 Materials and Methods

**2.1 Overview of the relevant temperature metrics.** The temperature of the land surface is

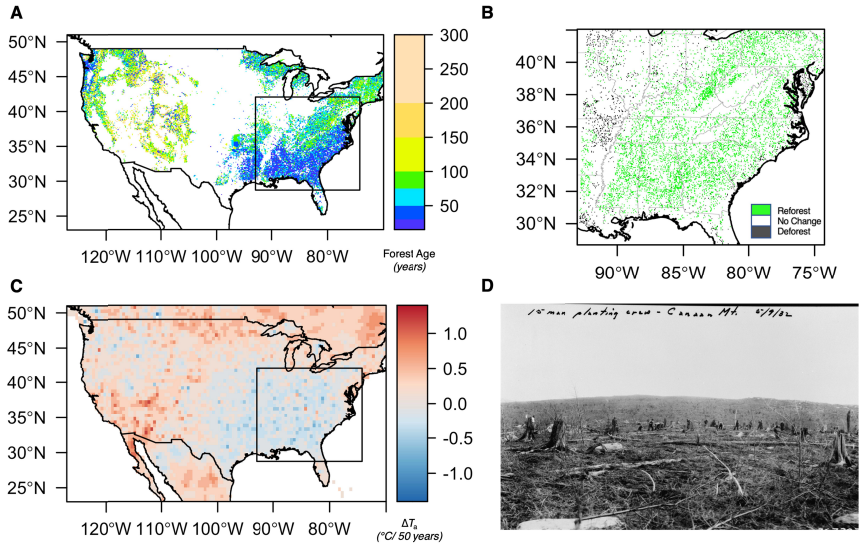


**Figure 1. The Southeastern United States' warming hole' and corresponding forest status**. (**A**) *Forest age estimates (1 km) as of 2019 calculated from forest age data from the North American Carbon Program.* (**B**) *Land conversion between agricultural land and forests from 1938 to 1992 calculated from 1 km FORE-SCE backcasting grids from the US Land Cover Trends project. The bounding box indicates the study area, and details on data sources are provided in the methods.* (**C**) *Trend in temperature change from 1900 to 2010 ($\Delta T_a$, °C/ 50 years) calculated using a season-trend model applied to 0.5° $T_a$ grids from University of Delaware monthly climatologies provided by the NOAA.* (***D***) *Historical photo of 15-person planting crew on 05/09/1932 in Tucker County, West Virginia. Original photo at the Forest Service Office in Elinks, WV. Obtained from https://www.loc.gov/pictures/resource/hhh.wv0307.photos.041150p/*

commonly used for assessing the biophysical impacts of land-cover change and is observable from both flux towers and remote sensing platforms. In terrestrial ecosystems, $T_s$ represents the temperature of the uppermost layer of vegetation, reflecting the outcome of the interactive effects of radiative transfer, leaf energy balance, eco-physiological controls on stomatal opening and closure, and aerodynamics. The $T_s$ is mechanistically connected to the near-surface $T_a$ through standard boundary layer theory for stratified flows. In vegetated systems, a thin layer of air called the roughness sublayer lies between the vegetation and the surface layer. Near-surface $T_a$ is generally measured (and modeled) at a height of 2 m above the surface, but vertical profiles of $T_a$ are influenced by canopy structural effects within the roughness sublayer. In short-stature ecosystems such as grasslands and croplands, the roughness sublayer is typically 1-2 meters thick, such that flux tower measurements of $T_a$ are typically made in the surface layer. Above forests with heights of 10 m or more, the roughness sublayer is much thicker (12-50 m), such that tower $T_a$ indicates the mean air temperature within the roughness sublayer, not the surface layer (Novick & Katul, 2020). Thus, comparing $T_a$ observations across forested and non-forested ecosystems is fraught with potential bias linked to canopy structural effects and measurement height. To overcome this limitation, we focus on two proxies for $T_a$ that are less sensitive structure effects on near-surface $T_a$ profiles, and that can be inferred from eddy covariance sensible heat flux tower data using methodologies described elsewhere (Novick & Katul, 2020). The first is the aerodynamic temperature ($T_{aero}$), which represents the air temperature within the upper reaches of the canopy. The second is the air temperature extrapolated aloft into the lower reach of the surface layer ($T_{extrap}$).

At regional scales, evaluating the impacts of land cover on $T_s$ requires a strategy to control for background variation in macroclimate. Here, the difference between MODIS $T_s$ and $T_a$ is evaluated, with the latter provided by the Daymet (Thornton et al., 2016) product ($T_{a,Daymet}$). Remotely sensed surface temperature is frequently termed 'Land Surface Temperature' (LST), but we use $T_s$ here for consistency with the other temperature metrics. Daymet interpolates data from meteorological weather stations, which are typically located over short grass surfaces, so it is viewed here as a 'reference' $T_a$ that is not influenced by variability in land cover. A summary of the temperature metrics used here can be found in Table S1.

**2.2 Forest age and land-cover change analyses.** Gridded 0.5 ° time series of monthly $T_a$ were obtained from the University of Delaware Air Temperature & Precipitation Dataset (Willmott & Matsuura, n.d.) provided by the NOAA/OAR/ESRL PSD, Boulder, Colorado, USA, from https://psl.noaa.gov. The gridded data are interpolated weather station data (Willmott & Matsuura, 1995), primarily from GHCN2 (Global Historical Climatology Network) observations and the GSOD (Global Surface Summary of Day) archive. Monthly mean air temperature (V4.01) was used to assess observed long-term changes in $T_a$ across the continental United States. Per-pixel temperature change in $T_a$ was estimated using a season-trend model (function 'STM') in the 'greenbrown' package (Forkel & Wutzler, 2015) for R (R Core Team, 2020). The season-trend model in 'greenbrown' is based on the additive decomposition model in refs (Verbesselt et al., 2010) and (Verbesselt et al., 2012). Harmonic and linear terms are used to model seasonal variation and trend, respectively, effectively 'detrending' the time series in a single step (Verbesselt et al., 2012).

To assess forest age, we obtained continental forest age maps from the North American Carbon Program (NACP), produced for the year 2006 (Y. Pan et al., 2012). Data were updated to give

accurate forest ages for 2019 by adding 13 years to all forest ages. This approach assumes that all forests continued to regrow and were not cut between 2006 (when the product was produced) and 2019. Although there are certainly locations for which this assumption will not hold, they generally represent a small fraction of the land surface and are mostly contained in the southeastern US where pine plantations are routinely harvested and replanted (Carman, 2013; Fig. S1).

To assess change in forest status (Fig.1B), land-cover change between 1938 to 1992 was calculated from 250 m FORE-SCE (FOREcasting SCEnarios of Land-use Change) backcasting grids from the US Land Cover Trends project (Sohl et al., 2007). Pixels were coded based on their land cover (cropland or forest), and per-pixel change was calculated between 1938 and 1992. To exclude sites that had undergone multiple conversions in the 20th century, an intermediate year, 1965, was also used. Pixels were classified into three categories: reforestation (change from cropland to forest), deforestation (forest to cropland), or 'no change' (land cover type was consistent in 1938, 1965, and 1992).

**2.3 Differences in $T_s$ -$T_a$ by land cover**. To compare relative surface cooling between different types of land cover on a regional scale, we used a remote sensing approach based on $T_s$ retrievals from the Moderate Imaging Resolution Spectroradiometer (MODIS; Wan et al., 2015) and $T_a$ estimates from the gridded 1 km Daymet product (Thornton et al., 2016). The MODIS Land Surface Temperature/Emissivity Daily Product (MYD11A1v6.1) has a spatial resolution of 1 km. The timing of the Aqua MODIS overpass (~1:30 pm local time) generally corresponds to the timing of daily maximum $T_s$ estimated from tower measurements (Fig. S2). Thus, to evaluate spatial variability in the difference between remotely sensed $T_s$, we corrected for macro-scale climate variability by subtracting $T_{a,Daymet}$ from MODIS $T_s$ :

$$T_s - T_{a,Daymet} = LST_{1:30pm,\ MYD11} - T_{a,Daymet} \quad (1)$$

If the near-surface air is warmer than the surface, $T_s$ -$T_a$ is negative; if the air is cooler than the surface, $T_s$ -$T_a$ is positive. Most often, especially at mid-day, the $T_s$ – $T_a$ will be positive (Mildrexler et al. 2011, Novick & Barnes *under review*), but we expect that it will be more negative (i.e., closer to zero) in forested versus non-forested sites. The monthly average $T_s$ - $T_{a,Daymet}$ for each 1 km pixel in the study area was obtained for each month from 2002 to 2018. The data presented in Figure 2 are the average monthly $T_s$ -$T_{a,Daymet}$ for the full time-series. The land cover type for each 1 km MODIS pixel was determined using the most recent 30 m National Land Cover Database (NLCD) land cover dataset (Dewitz, 2019). Mixed pixels that contained multiple land cover types at the 30 m level in each MODIS or Daymet 1 km pixel were classified as the most common land cover type in the pixel, provided that the most common land cover type comprised 70% or more of the pixel. There were relatively few pixels with grassland as the dominant land cover type, so we combined croplands and grasslands for the spatial $T_s$ -$T_{a,Daymet}$ maps (Fig. 2A, Figs S3-S5).

**2.4 Paired site flux tower analyses.** To understand reforestation effects on $T_s$ over the diurnal cycle (e.g., Fig. 2A, B), we used a paired site approach (Stoy et al. 2023), relying on observations from six forest-grassland site pairs in the study region. The site pairs are in Arkansas, North Carolina (3 pairs), Indiana, and New Hampshire (Table S2), and each paired set is separated by ~30 km or less. Site descriptions and details on eddy covariance data processing are provided elsewhere (Zhang et al., 2020); Briefly, all data were quality-controlled and gap-

filled using community-accepted standards embedded in the REddyProc processing tool (Wutzler et al., 2018). The $T_s$ data were inferred from the outgoing longwave radiation using the Stefan-Boltzmann law, with emissivity estimated as an empirical function of albedo following an established approach (Juang et al., 2007). The attribution of changes in $T_s$ to relevant mechanisms (i.e., variation in sensible versus latent heat flux) was accomplished through a Taylor-series expansion of the site-level energy balance equation, as described in detail in (Zhang et al., 2020), who presented results separately for each of the paired sites. In this study, those results are then aggregated across the site pairs.

The approach to estimate $T_{aero}$ and $T_{extrap}$ is described elsewhere (Novick & Katul, 2020). Briefly, $T_{aero}$ is determined by first quantifying the mean ratio between $T_s$ and the tower-measured $T_a$ ($XT$) when the measured sensible heat flux is near zero, implying that $T_a$ and $T_{aero}$ should be in equilibrium. The determination of $XT$ was performed for each hour of the day at each site separately for the peak of the growing season (June-Sep.) and the dormant season (Nov.-Mar.) and was then used to estimate $T_{aero}$ from the observed $T_s$ for every hourly or half-hourly observation period. The $T_{extrap}$ was then calculated assuming the logarithmic profiles from Monin-Obukhov Similarity Theory (Monin & Obukhov, 1954), forced with the estimated $T_{aero}$ and an estimate for the momentum roughness length for heat that varies as a function of measured friction velocity as described in (Novick & Katul, 2020). Here, results are shown for the temperature extrapolated into the first 10 meters of the surface layer after conceptually 'flattening' the ecosystems by replacing them with a rough surface characterized by two roughness heights: one for momentum absorption and one for heat transfer (see Novick & Katul, 2020 for details and code). This manuscript extends the results presented in Novick & Katul (2020) to the full set of paired sites in Table S3, noting that Novick & Katul only evaluate the results from the Duke Forest sites (in North Carolina).

The $T_a$ data presented in Figure 2 are mean air temperature data measured from a $T_a$/RH probe (such as the HMP35 or HMP45c, Vaisala) above the canopy, usually at or near the height of the EC systems (see Table S2).

**2.5 Broader synthesis of flux tower sites.** The 58 flux towers included in the broader synthesis (Fig. 3A-D) include the paired tower sites, as well as datasets acquired from the AmeriFlux network (Novick et al., 2018), and include towers installed and operated as part of the National Science Foundation's National Ecological Observatory Network (Metzger et al., 2019). The network data were limited to those that adopt a CC-BY-4.0 data use license. We first downloaded all available site-years from the network, excluding wetlands and irrigated croplands within the study region. Some sites and site-years were excluded due to missing information about radiative fluxes that are required to derive or calculate the temperature metrics. The towers retained for this analysis are described in Table S3. The same approaches used to determine $T_s$ , $T_{aero}$, and $T_{extrap}$ for the broader flux synthesis are the same as those described in section 2.4, with the exception that the AmeriFlux data were not gap-filled; rather, data were filtered to exclude those collected under very stable conditions in which turbulence generation is suppressed by buoyancy forces, and to exclude excessively large anomalous observation of sensible heat flux (i.e.,>1000 W/m$^2$). For the purposes of this paper, croplands managed as corn/soy rotations were treated as separate sites for corn and soy years. Estimates of canopy height and measurement height are required to calculate $T_{aero}$ and $T_{extrap}$. For most towers, they are available from the AmeriFlux Biological, Ancillary Disturbance, and Metadata (BADM) database; In cases where they were not available from the BADM, they were extracted from published studies. In rare

cases, a "best" guess was made based on known information about the canopy type or from site photos.

**2.6 Land Surface Temperature across forest/agriculture boundaries.** The NLCD was used to identify areas with adjacent forest:agriculture boundaries with a continuous extent of land cover on either side of the boundary. Transects were created across boundaries in the east/west direction at a ~90° angle. The transects were approximately 1 km long, with points every 10 m. In total, 44 transects were created in the study area (Fig. S6). We then extracted $T_s$ values from mid-summer clear-sky scenes (summer 2018) obtained from the Landsat Provisional Surface Temperature Product (Cook, 2014; Cook et al., 2014). Only one $T_s$ spatial profile was extracted for each transect, even if multiple images were available. The spatial resolution of Landsat imagery is 30 m, so the 10 m transects include several points within the same pixel. A smooth transition suggests that biophysical feedbacks on $T_s$ are linked to $T_a$ through advection and the formation of an internal boundary layer (Hsieh & Katul, 2009), since the surface itself is not mixed. For the lines in Figure 3E, we used a hyperbolic tangent function fit to each side of the transects (forest and agriculture). Distances were scaled from $-\pi$ to $\pi$ for fitting, then back-transformed for plotting.

**2.7 Impacts of Reforestation on Air Temperature***:* To investigate the impact of local land-cover change on long-term air temperature trends, we used monthly air temperature data from 398 United States Historical Climate Network (USHCN) meteorological stations. Meteorological stations, which were relatively evenly distributed across the study area (Fig. S8), allow us to associate locations more precisely with their land cover type compared to gridded temperature data. We evaluated the effects of land cover on annual temperature trends from 1900 to 2010 by focusing on both maximum temperatures during the growing season (June, July, August) and annual average temperatures. We did not conduct any interpolation of missing values.

We classified the weather stations based on the dominant land cover within a 500 m circular buffer surrounding each station, using 250 m FORE-SCE model backcasting grids. The classification was based on three time points (1938, 1965, and 1992), as described in section 2.2. Pixels were categorized as reforestation areas (change from agriculture to forest) if they were agricultural in 1938, converted to forest cover by 1965, and maintained as forested land until 1992, or if they were agricultural in both 1938 and 1965 but became forested by 1992. The areas predominantly surrounded by agriculture-to-forest conversion within 500 meters of the weather stations were defined as 'reforest' sites. Out of the 398 USHCN stations, 153 were predominantly surrounded by forest, 181 by agriculture, and 23 by reforestation. 41 of the sites underwent multiple land cover transitions or experienced deforestation in the 20$^{th}$ century.

To explore the impacts of reforestation on air temperature trends, we compared USHCN sites predominantly surrounded by reforestation to sites where the land cover remained stable as either agriculture or forest ('non-reforest') within a 50 km radius of the 'reforest' site. For each year, we calculated the temperature difference between the reforest site and non-reforest site (or sites) within the 50 km buffer. This approach builds upon the paired-site flux tower analyses described in section 2.4 by extending our understanding of the effects of reforestation on surface temperature to near-surface air temperature, covering a much longer period (back to the early 20th century), and including many more site 'pairs'. Our comparison of neighboring reforest and non-reforest site pairs included analysis of both growing-season maximum temperatures and

average annual temperatures. We excluded sites that had more than 5 years of missing data from 1900 – 2010. We had a total of 22 reforest sites and 44 non-reforest sites within 50 km of the reforest sites, resulting in 44 comparisons for annual average data and 42 comparisons for growing season data. The lower number of growing season comparisons is due to missing data for two sites. The reforest sites had a median of two non-reforest sites within a 50 km radius. We based the 50 km radius on a previous study that showed changes in maximum air temperature up to 50 km away from the site of land cover change (Cohn et al., 2019).

**2.8 Exploring the links between forest age and air temperature change within the Warming Hole.** To further investigate the influence of reforestation on the warming hole, we examined the relationship between forest age and recent growing season trends in $T_a$ at the regional scale (Fig. 4D). To align our recent 'snapshot' of forest age with $T_a$, we compared the 1 km NACP-derived forest age maps with recent trends (1970-present) in $T_a$ from the University of Delaware climatologies (Willmott & Matsuura, n.d.). We used the season-trend approach described in section 2.2 to estimate the slope of trends in annual $T_a$ time-series from 1970-2017 (Fig. 4D). The slope of the temperature change from 1970-present, $\Delta T_a$ , was calculated for each pixel, and forest age data were aggregated to the coarser scale of the $T_a$ data (Fig. S1B) using a mode function, "modal", in the 'raster' R package (Hijmans, n.d.), and then resampled using nearest neighbor interpolation. Then, we calculated focal correlations between aggregated forest age (Fig. S1B) and temperature trends, specifically, a simple moving window correlation between $\Delta T_a$ from 1970-present and forest age in a 5 x 5 window using the 'raster correlation' function in the 'SpatialEco' R package (Evans, 2021).

We note that although gridded daily microscale (1 km) $T_a$ products such as Daymet should be relatively insensitive to local impacts of land cover on $T_a$ (Fig. S7), the fingerprint of reforestation may be detectable from coarser yearly mesoscale $T_a$ estimates at 0.5-degree resolution. Observational and modeling studies support regional-scale impacts of land cover change on mesoscale $T_a$ (Bonan, 2001; Mahmood et al., 2014), providing further justification for our approach.

## 3 Results

Across the study area, the difference between $T_s$ and the $T_{a,Daymet}$ was more negative for forests than grasslands and croplands most of the time (Fig. 2). Since the $T_{a,Daymet}$ normalizes for macro-scale temperature variability, this result implies that forest surfaces are cooler than the surfaces of nearby grasslands and croplands by the same amount. The effect was most pronounced during the growing season, when forests were cooler than non-forests by an average of 0.5-2 ° C (Fig. 2A, B), with smaller reductions observed in spring and fall.

Next, we leveraged rich surface energy balance information from eddy covariance (EC) flux towers, beginning with six co-located ('paired') forest and grassland sites in the study region (Table S2; Zhang et al., 2020). Across these paired sites, forest $T_s$ was 4-5 °C cooler, on average, than nearby grasslands during midday periods (Fig. 2D, E), driven primarily by enhanced evapotranspiration in summer and enhanced sensible heat flux in winter that outweighed albedo-driven warming effects in the darker forests (Zhang et al., 2020).

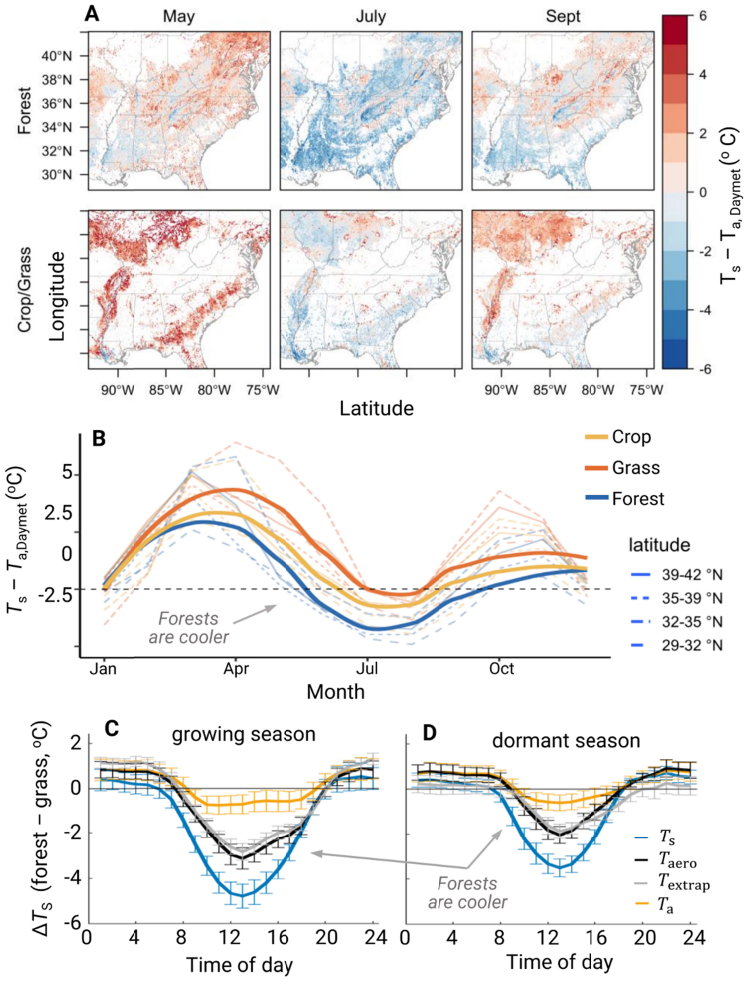


**Figure 2. A forest surface cooling effect is evident in both MODIS and flux tower (A-B) observations (C, D).** (**A**) *Average difference between daily ~1:30 pm surface temperature* ($T_s$) *and daily maximum air temperature* ($T_{a,\ Daymet}$) *for 2003-2018 for forests* (*top row*) *and combined grasslands and croplands* (*'other', second row*). *Negative values indicate cooler surface than air temperature* (*surface cooling*) *and positive values indicate warmer surface air temperature.* (**B**) *The seasonal cycle of* $T_s$ - $T_{a,Daymet}$ *for forests* (*blue*), *grasslands* (*yellow*), *and croplands* (*orange*) *for the study region* (*bolded lines*), *with latitude ranges indicated by faint dashed lines.* (**C**) *Remotely sensed surface temperature* ($T_s$), *corrected by the* $T_{a,\ Daymet}$ *reference, shown as a function of forest age, using July data for the period 2003-2018.* (**D, E**) *Diurnal time series of the difference between forest and grassland* $T_s$ (*blue*), $T_{aero}$ (*black*), $T_{extrap}$ (*gray*), *and tower-measured* $T_a$ (*yellow*) *for six eddy covariance site pairs* (*Table S3*) *for the growing season* (**D**) *and the dormant season* (**E**).

Although the paired-site approach represents a 'gold standard' for understanding the biophysical impacts of land-cover change (Zhang et al., 2020), only a handful of forest-grassland flux tower pairs exist. To expand the scope of inference, we synthesized $T_s$ observations from 58 Ameriflux EC tower sites across the EUS, again correcting for macro-scale climate variability with $T_{a,Daymet}$ (Table S3). The results revealed widespread daytime surface cooling in forests compared to non-forests (Fig. 3A). The difference between tower-derived $T_s$ and the reference $T_{a,Daymet}$ was 4.5-5.5 ° C lower for forests than grasslands during the growing season (Fig. 3A). When comparing forests to croplands, $T_s$ was more similar than for grasslands, but tall forests were still relatively cooler than croplands (Fig. 3A).

**3.1 Land cover effects on near-surface $T_a$**. For the surface cooling to extend beyond the stand-scale and thus contribute to the warming hole, changes in $T_s$ must translate to changes in near-surface $T_a$.

We adopted several new or emerging approaches to quantify the extent to which the forest cooling effects on $T_s$ extend to $T_a$. First, we harnessed flux tower data to estimate metrics of $T_a$ that are less sensitive to canopy effects (11): $T_{aero}$ and $T_{extrap}$ (Table S1). In the paired sites and across the regional network of flux towers, the midday growing season $T_{aero}$ and $T_{extrap}$ are cooler for forests than for grasslands (Fig. 2D, E, and 3A-D). Consistent with expectations, forests have the strongest cooling effect on surface temperatures (Fig. 3A) and smaller effects on air temperatures (Fig. 3B-D). $T_{aero}$ and $T_{extrap}$ were similar between forests and croplands, although $T_{aero}$ was substantially lower for tall forest stands (Fig. 3B-D). Despite the confounding influence of canopy effects on near-surface $T_a$ profiles, tower-measured $T_a$ also suggests a cooling effect of forests, although differences across biomes were smaller (Fig. 3D).

Next, to provide an independent perspective on surface and air temperature coupling, we used high-resolution (30 m) Landsat $T_s$ retrievals to evaluate the extent to which transitions in $T_s$ at forest-cropland boundaries were smooth or abrupt (Fig. 3E; Fig. S6). A relatively smooth temperature transition from cooler forests to warmer croplands was observed (Fig. 3E) that extends over length scales of several hundred meters.

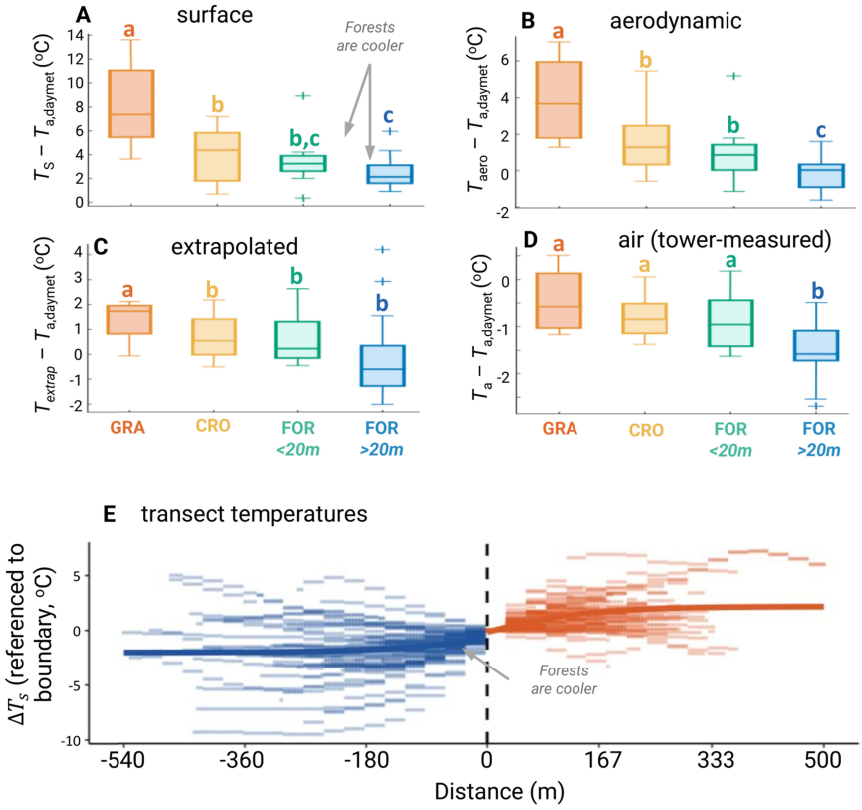


**Figure 3: Extension of surface cooling to the near-surface air.** (**A-D**) *Difference in tower-measured or derived temperature metrics and reference* $T_{a,\ Daymet}$. *Each boxplot shows the monthly midday growing season site-level means, with forested ecosystems split by canopy height* (≤*20 m or >20 m*). *Horizontal lines indicate the median, boxes indicate the interquartile range, whiskers indicate the data range* (=*1.5 times the interquartile range*), *and the symbols' +' indicate outliers. Letters indicate significant differences between groups evaluated using a two-sample t-test at a significance level of p = 0.05. Note the y-axis range varies between panels. Each panel is informed by data from 13 grass towers, 19 cropland towers, 10 towers in forests <20m tall, and 16 towers in forests >20m tall.* (**E**) *Horizontal profiles* ("*transects*") *of* $T_s$ *across the forest:cropland boundary. Values of* $\Delta T_s$ (*sampled every 10 m*) *are relative to the temperature at the forest:cropland boundary. Negative values of* $\Delta T_s$ *indicate lower temperatures than at the boundary, and positive values of* $\Delta T_s$ *indicate higher temperatures than at the boundary. Points left of the zero-distance line indicate forest* (*blue*), *and points right of the zero-distance line indicate agricultural croplands* (*orange*). *The blue and orange lines indicate a hyperbolic tangent function fit to the pooled transect data.*

387

**3.2 Evaluating the signatures of land-cover change in long-term meteorological observations**. To evaluate the signatures of land-cover change in long-term meteorological observations, we compared long-term records of air temperature from weather station sites, estimates of forest age, and gridded air temperature data. First, we examined the long-term temperature trends from 398 USHCN sites in the study region. Our analysis showed that temperatures remained relatively stable throughout the 20th century, with a decline in average temperatures in the late 1950s (Fig. 4A). Next, w**e** investigated the cooling effect of regrowing forests by analyzing the difference between $T_s$ and the reference $T_{a,Daymet}$ as a function of forest age. Results indicated that the cooling effect was strongest for forests around 25 years old, as the difference reached its lowest point at that age (Fig. 4B).

To further explore the cooling effect of reforestation, we compared 10-year rolling means of $T_a$ from historical USHCN stations in sites predominantly surrounded by reforestation ('reforest') and neighboring sites that did not undergo land cover conversion ('non-reforest') within 50 km. In terms of average annual temperatures, reforested sites were consistently cooler than their non-reforesting counterparts throughout the 20th century (Fig. 4B, blue line). The results were more nuanced for maximum growing season temperatures. Sites with nearby reforestation tended to be warmer in the early half of the 20th century and cooler in the latter half, and the magnitude of this cooling effect increased throughout the study period. By the end of the 20th century, reforesting sites were up to 1 °C cooler than their non-reforesting neighbors in terms of maximum growing season air temperatures (Fig. 4B, red line).

Finally, to explore the relationship between forest age and temperature trends, we explored spatial variation in the correlation between decadal-scale growing season $T_a$ trends (from University of Delaware 0.5° monthly climatologies) and forest age across the continental US (Fig. 4D). A positive correlation coefficient indicates that pixels dominated by younger forests (i.e., < 100 years as of 2019) experienced less warming during this period than pixels dominated by more mature stands (see inset to Fig. 4D). This correlation coefficient was positive across much of the study region on the annual timescale (63% of pixels; Fig. 4D), and when considering growing season temperature trends alone (Fig. S9B), consistent with the expectation that reforesting areas experience less warming. However, there is substantial variability across the study region, with negative relations between forest age and $\Delta T_a$ observed, including in the central Appalachians and Ozarks.

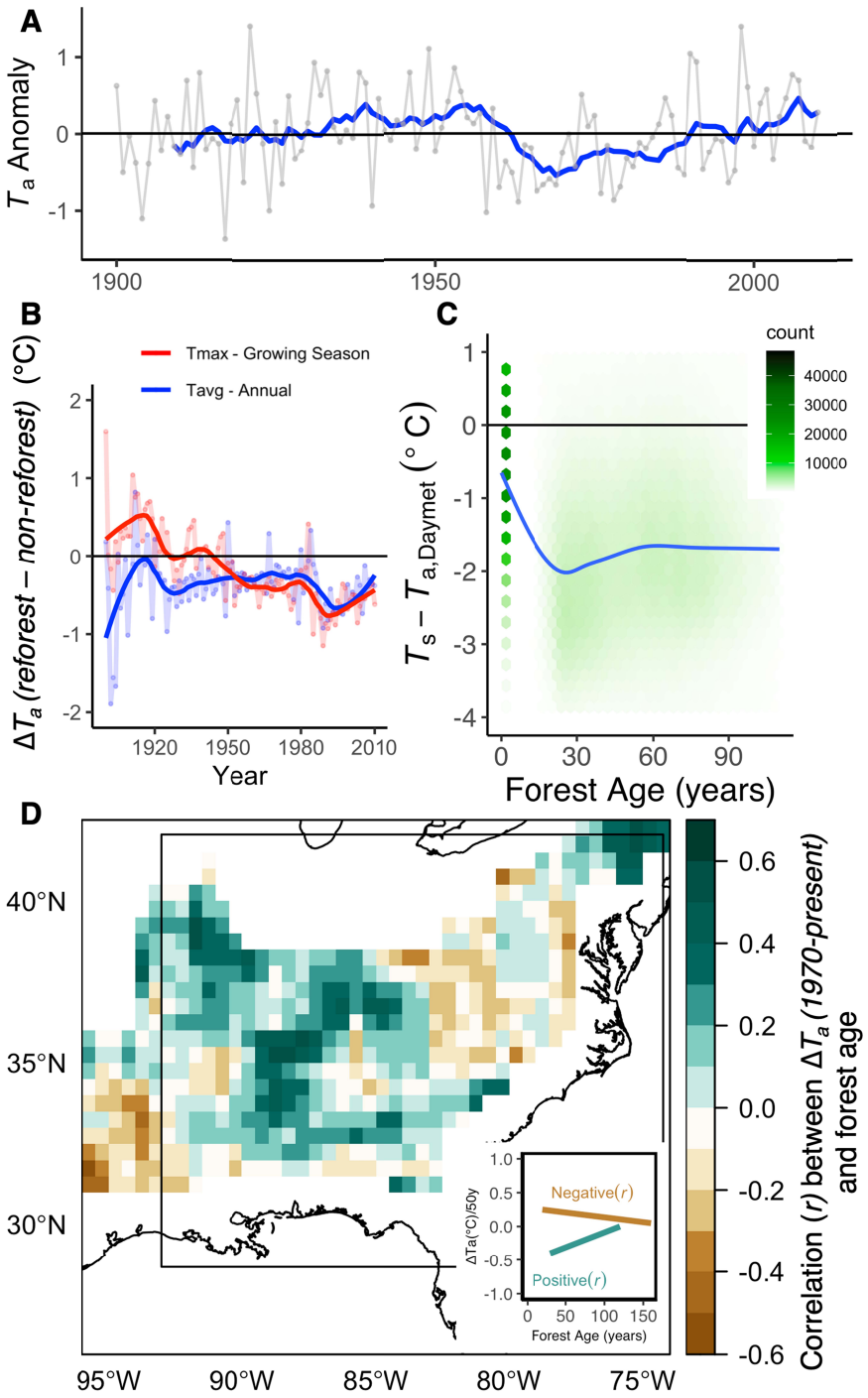


**Figure 4. Relationships between land cover, long-term temperature trends, and forest age.** (**A**) *Average long-term trend in pooled annual $T_a$ anomalies for 398 USHCN sites in the EUS. The blue line represents the 10-year moving average.* **(B)** *Difference in air temperature between USCHN sites predominantly surrounded by reforestation and non-reforesting sites located within a 50 km radius, presented as 10-year moving averages. The red line shows the difference in summer maximum temperatures, and the blue line shows the difference in average annual temperatures. Negative values indicate that the reforesting site was cooler than its neighboring non-reforesting site(s).* **(C)** *Remotely sensed July surface temperature ($T_s$) corrected by the $T_{a,\text{Daymet}}$ reference displayed as a function of forest age for the period 2003-2018.* (***D***) *Spatial moving window correlation (5 x 5 window) between forest age and recent long-term $T_a$ trends (1970-present). A negative correlation indicates older forests are associated with greater cooling, and a positive correlation indicates younger forests are associated with greater cooling (inset).*

419

## 4 Discussion and Conclusions

Our study provides strong evidence that reforestation has biophysical climate benefits in the EUS and demonstrates a clear relationship between observed land-cover change and observed temperature changes. Taken together, our findings indicate reforestation has a cooling effect on surface and near-surface air temperature in the EUS, and likely contributed to the slower pace of warming in the region. Both ground- and satellite-based observations indicate that EUS forests cool the land surface by 1-2 °C annually (Fig. 2) compared to nearby surfaces with short-stature vegetation. During midday in the growing season, surface cooling is 2 to 5 °C (Fig. 2C, Fig. 3A), and forests aged 25-50 years exhibit the strongest cooling effect (Fig. 4C). The surface cooling extends to the near-surface air, with forests reducing midday growing-season air temperature by up to 1 °C (Fig. 3D, Fig. 4B). Historical weather station data and regional-scale gridded long-term air temperature data analyses establish a link between reforestation and the observed lack of warming in the EUS (Figure 4). In particular, weather stations located near reforesting areas recorded temperatures that were 0.5 – 1.0 °C cooler than stations surrounded by land that experienced little change in forest cover. Overall, these results highlight the substantial adaptation potential of reforestation as a natural climate solution.

**4.1 Assessing land cover impacts on surface and near-surface air temperature.** Assessing the direct consequence of land-cover change on surface temperature is relatively straightforward, given the abundance of satellite observations of $T_s$ and complementary measurements of surface energy fluxes from ground-based towers. We have known for some time that reforestation tends to increase $T_s$ in the boreal zone (due to large reductions in albedo, Bright et al., 2017; Swann et al., 2010) and decreases $T_s$ in the tropics (due to enhanced latent heat fluxes, Bonan, 2008). In this study of temperate ecosystems, satellite and flux tower data are combined to demonstrate that, in mid-latitude forests of the eastern US, forest-driven reductions to $T_s$ are: (1) 2-5 °C at midday during the growing season (Fig. 2, Fig. 3A), (2) achievable within ~25 years of forest regeneration (Fig. 4C), and (3) stable across mature forest classes (Fig. 2C). These results, combined with other recent work on the topic, contribute to a growing consensus that reforestation tends to have a direct cooling effect on $T_s$ across much of the temperate zone.

Assessing the impact of land cover change on near-surface air temperature is more challenging due to technical and methodological limitations. Yet, understanding the potential of reforestation and other natural climate solutions to confer climate adaptation benefits requires that we quantify land cover impacts on near-surface air temperature. Furthermore, for the surface cooling to extend beyond the stand scale and thus contribute to the warming hole, changes in $T_s$ must translate to changes in $T_a$. In turn, evaluating the impacts of land cover on near-surface air temperatures requires overcoming technical and methodological challenges, including data scarcity and canopy structural effects that prevent straightforward comparisons of air temperature measured above different ecosystems. We adopted several new or emerging approaches to overcome the technical and methodological challenges associated with evaluating $T_a$.

First, we harnessed flux tower data to estimate metrics of $T_a$ that are less sensitive to canopy effects. By relying on proxies for near-surface air temperature that are relatively insensitive to canopy structural effects (e.g., $T_{aero}$ and $T_{extrap}$), we demonstrate that, across much of the study region, the cooling effect of forests on $T_s$ extends to the near-surface air temperature above the

canopy (Fig. 2E, F; Figs. 3A-D). Forest cover impacts on $T_a$ are smaller than impacts on $T_s$ (~ 1 °C for midday growing season periods, Fig. 2D, Fig. 3) but still consequential, particularly compared to the magnitude of historic and predicted changes in $T_a$ due to climate change.

Next, to provide an independent perspective on surface and air temperature coupling, we used high-resolution (30 m) Landsat $T_s$ retrievals to evaluate the extent to which transitions in $T_s$ at forest-cropland boundaries were smooth or abrupt. A smoother transition suggests that biophysical feedbacks on $T_s$ are linked to $T_a$ through the formation of an internal boundary layer, assuming the thermal inertia of leaves is small. A relatively smooth temperature transition from cooler forests to warmer croplands was observed (Fig. 3E) that extends over length scales typical of adjustment distances needed for the equilibration of the air temperature internal boundary layer. Furthermore, the smooth transition of $T_s$ across forest-grassland boundaries implies coupling between $T_s$ and $T_a$ that extends at least several hundred meters beyond the ecosystem boundary. This result helps to confirm previous theoretical modeling (Hsieh & Katul, 2009; Li & Wang, 2019) and augments a similar exercise in the tropics (Cohn et al., 2019) by documenting these processes at a large spatial scale over much of the EUS. Importantly, it is over this distance that biophysical impacts on $T_a$ are substantial enough to feedback on $T_s$. It is likely that reforestation impacts on $T_a$ extend further, but beyond a few hundred meters are not great enough to drive significant changes in grassland $T_s$.

Our analyses have shown that forests in the EUS exert a cooling effect on both surface and air temperatures, and that this effect can extend across ecosystem boundaries. Importantly, this cooling benefit is most pronounced during midday summer periods (Fig. 2C, D; Fig. 4B), which are typically associated with high heat stress and extreme events. These findings suggest that, in temperate zones, reforestation may provide the greatest climate adaptation benefit precisely when it is most needed.

**4.2 Linking reforestation to the observed lack of warming in the Eastern US.** To establish a link between reforestation and the observed lack of warming in the EUS, we analyzed historical weather station data to associate near-surface air temperature records with land cover changes during the 20th century. Additionally, we conducted a regional-scale analysis to investigate the relationship between spatial patterns of reforestation and temperature patterns in the EUS.

Overall, our analysis of long-term $T_a$ records from 398 USHCN weather stations is consistent with the general understanding of 20$^{th}$ temperature trends in the EUS as it reveals no overall warming trend (Fig. 1B; Fig. 4A). We observed a sharp decrease in average temperatures in the 1950s, which corresponds with previous studies that found an abrupt climactic regime shift in 1957-1958 in the EUS (Partridge et al., 2018; Rogers, 2013). The causes of this abrupt, uniform cooling are likely multifaceted. The abrupt cooling could be related to changes in jet stream position, specifically sharp decreases in the Meridional Circulation Index (MCI; Tosca et al., 2017). However, the impact of decreases in the MCI is greater on winter temperatures, which decreased more uniformly during the twentieth century than summer temperatures (Fig. S10). Therefore, focusing on summer temperature time-series in addition to annual temperature time-series can help to distinguish the influence of the MCI from other mechanisms, including reforestation.

We investigated the signatures of reforestation in long-term climate data by analyzing the difference in long-term $T_a$ records between weather stations predominantly surrounded by reforestation and nearby (within 50 km) weather stations that did not undergo land cover change (remained agriculture or forest) throughout the 20th century. In the early 20th century, we found that sites with nearby reforestation tended to be warmer than sites without reforestation in terms of maximum daily growing season temperatures (Fig. 4B), which is consistent with expectations if these areas were sparsely vegetated at the time (Fig. 1). However, as the 20th century progressed, sites predominantly surrounded by reforestation became increasingly cool relative to their non-reforesting neighbors within 50 km. By the end of the 20th century, reforesting sites were up to 1 °C cooler than their non-reforesting neighbors in terms of maximum growing season air temperatures (Fig. 4B). The magnitude of the cooling effect is consistent with the results from the tower air temperature comparisons (Fig. 2D, Fig. 3), providing independent evidence of the impact of reforestation on near-surface air temperature.

Analysis of the forest cooling by age indicated that the cooling effect of regrowing forests takes about 25 years to fully develop, with forests around 25 years old exhibiting the strongest cooling effect (Fig. 4C). This time frame is consistent with the time it takes for regenerating forests in the region to achieve levels of hydrological function comparable to mature forests (Ford et al., 2011). During the growing season, when the cooling impact of regrowing forests is expected to be strongest, reforesting sites were consistently cooler than nearby non-reforesting sites by the late 1950s (Fig. 4B), which roughly corresponds to forests aged 20-30 years if we consider the widespread agricultural abandonment and federal reforestation efforts in the 1930s as age zero (e.g., Fig. 4D). The trends in maximum growing season temperature increased throughout the 20$^{th}$ century, supporting the idea that as forests grew, the summer cooling effect increased (Fig. 4B).

Regional-scale analysis of gridded long-term air temperature data provided an independent, complementary approach to the weather station analyses. The analysis showed that younger forests were associated with lower historic rates of warming across most of the study region (Fig. 4D). This finding, combined with the weather station analyses, suggests that reforestation had a cooling effect on near-surface air temperature across a wide swath of the EUS. Parsing the trends in long-term $T_a$ time series as a function of land cover and historic land-cover change (e.g., the results in Figure 4) captures both the influence of regional-scale non-local effects and the finer-scale direct effects. While uncertainties remain regarding the characterization of forest age and historical land cover, our results support the expectation that 20th-century EUS reforestation had a net cooling effect that extended well beyond the surface and local stand-scale. For weather stations located near to, but outside of, reforested areas, the effect amounts to a suppression of $T_a$ on the order of 0.5 – 1 $^{o}$C for the latter half of the 20$^{th}$ century.

**4.3 Non-local effects of land-use change.** A more holistic perspective on the efficacy of nature-based climate solutions accounts for the possibility that local (e.g., ecosystem-scale) changes in land cover can initiate non-local impacts over much broader scales (Swann et al., 2012; Williams et al., 2021). For example, reforestation can lead to increased evapotranspiration, resulting in increased cloud cover and precipitation (Cerasoli et al., 2021; Manoli et al., 2016) that extend across the landscape, which would tend to amplify local cooling effects, particularly during the daytime. Localized land-cover changes can also cause shifts in atmospheric circulation, which can have continental or even global-scale consequences for temperature, precipitation,

549 cloudiness, and other meteorological drivers (Pongratz et al., 2010; Swann et al., 2012; Winckler
550 et al., 2019). Earth system models have been the primary tool for exploring these
551 teleconnections, with many studies suggesting a dramatic role for non-local processes to amplify
552 or counteract the local impacts of land-cover change on surface and near-surface temperature.
553 However, results from these modeling studies are sometimes contradictory, and the difference
554 between model predictions and observations can be large (Bonan, 2008; De Hertog et al., 2022).

555 This study employs observational approaches to indirectly assess the non-local effects of land-
556 cover change. We investigate how surface temperature effects can extend to the air and be
557 transported across the landscape, providing a generalizable method to investigate these
558 connections. Our approach includes exploring gradients in surface temperature ($T_s$) across
559 ecosystem boundaries, as shown in Figure 3, to uncover the potential local extent of such effects.
560 This connection is crucial because long-term records of air temperature, which are used to
561 delineate the warming hole, are made in open clearings. By uncovering how surface temperature
562 effects extend to the air, we can gain insight into how local changes in land cover may initiate
563 non-local impacts across much broader scales. It is important to note that these observational
564 approaches have limitations, as they cannot fully account for the possibility that non-local effects
565 of land-use change within and outside the study region are influencing long-term temperature
566 trends in the EUS.
567
568 For example, changes in agricultural management, such as agricultural intensification and
569 increased irrigation use, are known to have a local cooling effect (Mueller et al., 2016), and
570 many areas of the EUS have experienced these management shifts (Spangler et al., 2020).
571 Changes in agricultural management that promote cooling could obscure the influence of
572 reforestation in the comparison of long-term trends from forested and cropland ecosystems (e.g.,
573 Figure 4). Thus, the results presented here can be considered conservative. It is also possible that
574 land-use changes occurring well outside of the study region may be driving widespread trends in
575 long-term temperature trends in the EUS via teleconnections (Swann et al., 2018), or that certain
576 non-local temperature effects of reforestation or deforestation may be opposite in sign to the
577 local effects (De Hertog et al., 2022; Pongratz et al., 2021). These non-local teleconnections are
578 currently only possible to explore with modeling studies that tend to rely on idealized
579 experiments that force instantaneous and extreme changes in land cover across broad regions.
580 Evaluating all modes of historical land-use change that might have affected climate in the EUS
581 would be computationally expensive (if not impossible) and would still be unlikely to resolve,
582 with precision, the relatively small changes in $T_s$ and $T_a$ that are revealed by our observation-
583 driven approach.
584

585 **4.4 Conclusions.** Various hypotheses have been proposed to explain the observed lack of 20th-
586 century warming in the eastern United States (e.g., Meehl et al., 2012; Z. Pan et al., 2004;
587 Partridge et al., 2018; Tosca et al., 2017). Our work does not identify widespread reforestation as
588 the sole factor causing the EUS warming hole or its trend, but multiple independent data sources
589 suggest it may have been an important contributor to this lack of historic regional warming.
590 Beyond that, our study provides robust evidence of local biophysical climate benefits of
591 reforestation in the EUS. The strong and persistent increase in forest cover throughout the region
592 in the 20$^{th}$ century contributed to cooling, which is consistent with observed temperature

changes. In addition, our findings demonstrate that reforestation has a consistent cooling effect on both surface and air temperatures, especially during midsummer periods when high temperatures can be most harmful. These findings emphasize the potential for reforestation to provide local climate adaptation benefits in temperate regions such as the EUS, highlighting the importance of biophysical co-benefits of nature-based climate solutions.

**Acknowledgments**

The authors acknowledge Mike Voyles, Michael Benson, Steve Scott, Koong Yi, Matt Wenzel, and Chris Sobek for their help in installing and maintaining the paired flux tower sites. The findings and conclusions in this publication are those of the authors and should not be construed to represent any official USDA or US Government determination or policy. The authors declare no competing interests. Funding was provided by the US National Science Foundation (NSF) grant through grants NSF-DEB-1552747, NSF-DEB-1637522, NSF-IOS-1754893, and NSF-AGS-2028633. KAN and ACO also acknowledge support from the USDA Forest Service – Southern Research Station. GK acknowledges support from the US Department of Energy (DOE) Office of Science (DE-SC0022072). QZ acknowledges support from the National Natural Science Foundation of China (U2243214). Funding for the AmeriFlux data portal was provided by the DOE Office of Science. This material is based in part on work supported by the NSF through the National Ecological Observatory Network (NEON) program. The authors thank the AmeriFlux tower PIs for generously sharing their data. The authors declare no conflicts of interest.

**Open Research**

The data used in this study are freely accessible. The AmeriFlux tower data are available from the AmeriFlux data portal (https://ameriflux.lbl.gov/), and the various remote sensing and meteorological network data are available from links and repositories described in the methods section. To ensure reproducibility, we will make intermediate data products, code, and transformed data products (i.e., those derived from raw publicly available data) publicly available on a Dryad repository prior to publication of this manuscript. The Dryad repository will have a persistent DOI identifier to ensure accessibility and citation. If site data are not yet available for download via AmeriFlux at the time of publication, we will include the raw data in our Dryad repository.

***Data are available for peer-reviewers at the following Dryad repository:***
https://datadryad.org/stash/share/Xc8kjs7DMNAeTdHFfTLWC2gTXV3zip8ZMxTN3N-6mdQ

To facilitate access to the data, we will provide direct links to the data or detailed instructions on how to access the data efficiently. We will also follow any acknowledgments or citation guidelines provided by the repository or data/software source when creating our final Availability Statement and referencing the data in our References section.

633 **References**

634 Anderson, R. G., Canadell, J. G., Randerson, J. T., Jackson, R. B., Hungate, B. A., Baldocchi,
635 D. D., et al. (2011). Biophysical considerations in forestry for climate protection.
636 *Frontiers in Ecology and the Environment*, *9*(3), 174–182.
637 https://doi.org/10.1890/090179
638 Baldocchi, D., & Ma, S. (2013). How will land use affect air temperature in the surface boundary
639 layer? Lessons learned from a comparative study on the energy balance of an oak
640 savanna and annual grassland in California, USA. *Tellus B: Chemical and Physical*
641 *Meteorology*, *65*(1), 19994. https://doi.org/10.3402/tellusb.v65i0.19994
642 Bonan, G. B. (2001). Observational Evidence for Reduction of Daily Maximum Temperature by
643 Croplands in the Midwest United States. *Journal of Climate*, *14*(11), 2430–2442.
644 https://doi.org/10.1175/1520-0442(2001)014<2430:OEFROD>2.0.CO;2
645 Bonan, G. B. (2008). Forests and Climate Change: Forcings, Feedbacks, and the Climate
646 Benefits of Forests. *Science*, *320*(5882), 1444–1449.
647 https://doi.org/10.1126/science.1155121
648 Bright, R. M., Davin, E., O'Halloran, T., Pongratz, J., Zhao, K., & Cescatti, A. (2017). Local
649 temperature response to land cover and management change driven by non-radiative
650 processes. *Nature Climate Change*, *7*(4), 296–302. https://doi.org/10.1038/nclimate3250
651 Carman, S. F. (2013). Indiana forest management history and practices. In: Swihart, Robert K.;
652 Saunders, Michael R.; Kalb, Rebecca A.; Haulton, G. Scott; Michler, Charles H., eds.
653 The Hardwood Ecosystem Experiment: a framework for studying responses to forest
654 management. USDA Forest Service Gen. Tech. Rep. NRS-P-108, 12-23. Retrieved from
655 https://www.nrs.fs.fed.us/pubs/42897
656 Cerasoli, S., Yin, J., & Porporato, A. (2021). Cloud cooling effects of afforestation and
657 reforestation at midlatitudes. *Proceedings of the National Academy of Sciences*, *118*(33),
658 e2026241118. https://doi.org/10.1073/pnas.2026241118
659 Cohn, A. S., Bhattarai, N., Campolo, J., Crompton, O., Dralle, D., Duncan, J., & Thompson, S.
660 (2019). Forest loss in Brazil increases maximum temperatures within 50 km.
661 *Environmental Research Letters*, *14*(8), 084047. https://doi.org/10.1088/1748-
662 9326/ab31fb
663 Cook, M. (2014). Atmospheric Compensation for a Landsat Land Surface Temperature Product.
664 *Theses*. Retrieved from https://scholarworks.rit.edu/theses/8513
665 Cook, M., Schott, J. R., Mandel, J., & Raqueno, N. (2014). Development of an Operational
666 Calibration Methodology for the Landsat Thermal Data Archive and Initial Testing of the
667 Atmospheric Compensation Component of a Land Surface Temperature (LST) Product
668 from the Archive. *Remote Sensing*, *6*(11), 11244–11266.
669 https://doi.org/10.3390/rs61111244
670 De Hertog, S. J., Havermann, F., Vanderkelen, I., Guo, S., Luo, F., Manola, I., et al. (2022). The
671 biogeophysical effects of idealized land cover and land management changes in Earth
672 system models. *Earth System Dynamics*, *13*(3), 1305–1350. https://doi.org/10.5194/esd-
673 13-1305-2022
674 Dewitz, J. (2019). National Land Cover Dataset (NLCD) 2016 Products [Data set]. U.S.
675 Geological Survey. https://doi.org/10.5066/P96HHBIE
676 Evans, J. S. (2021). spatialEco. R package version 1.3-6. Retrieved from
677 https://github.com/jeffreyevans/spatialEco.

678 Farella, M. M., Fisher, J. B., Jiao, W., Key, K. B., & Barnes, M. L. (2022). Thermal remote
679 sensing for plant ecology from leaf to globe. *Journal of Ecology*, 1365-2745.13957.
680 https://doi.org/10.1111/1365-2745.13957
681 Ford, C. R., Laseter, S. H., Swank, W. T., & Vose, J. M. (2011). Can forest management be used
682 to sustain water-based ecosystem services in the face of climate change? *Ecological*
683 *Applications*, *21*(6), 2049–2067. https://doi.org/10.1890/10-2246.1
684 Forkel, M., & Wutzler, T. (2015, April 15). greenbrown - land surface phenology and trend
685 analysis. A package for the R software. (Version 2.2). Retrieved from
686 http://greenbrown.r-forge.r-project.org/
687 Griscom, B. W., Adams, J., Ellis, P. W., Houghton, R. A., Lomax, G., Miteva, D. A., et al.
688 (2017). Natural climate solutions. *Proceedings of the National Academy of Sciences*,
689 *114*(44), 11645–11650. https://doi.org/10.1073/pnas.1710465114
690 Hall, B., Motzkin, G., Foster, D. R., Syfert, M., & Burk, J. (2002). Three hundred years of forest
691 and land-use change in Massachusetts, USA. *Journal of Biogeography*, *29*(10–11), 1319–
692 1335. https://doi.org/10.1046/j.1365-2699.2002.00790.x
693 Helbig, M., Gerken, T., Beamesderfer, E. R., Baldocchi, D. D., Banerjee, T., Biraud, S. C., et al.
694 (2021). Integrating continuous atmospheric boundary layer and tower-based flux
695 measurements to advance understanding of land-atmosphere interactions. *Agricultural*
696 *and Forest Meteorology*, *307*, 108509. https://doi.org/10.1016/j.agrformet.2021.108509
697 Hijmans, R. (n.d.). raster: Geographic Data Analysis and Modeling. R package version 3.5-9.
698 Retrieved from https://CRAN.R-project.org/package=raster
699 Houghton, R. A., & Hackler, J. L. (2000). Changes in terrestrial carbon storage in the United
700 States. 1: The roles of agriculture and forestry. *Global Ecology and Biogeography*, *9*(2),
701 125–144. https://doi.org/10.1046/j.1365-2699.2000.00166.x
702 Hsieh, C.-I., & Katul, G. (2009). The Lagrangian stochastic model for estimating footprint and
703 water vapor fluxes over inhomogeneous surfaces. *International Journal of*
704 *Biometeorology*, *53*(1), 87–100. https://doi.org/10.1007/s00484-008-0193-0
705 Juang, J.-Y., Katul, G., Siqueira, M., Stoy, P., & Novick, K. (2007). Separating the effects of
706 albedo from eco-physiological changes on surface temperature along a successional
707 chronosequence in the southeastern United States. *Geophysical Research Letters*, *34*(21),
708 L21408. https://doi.org/10.1029/2007GL031296
709 Lee, X., Goulden, M. L., Hollinger, D. Y., Barr, A., Black, T. A., Bohrer, G., et al. (2011).
710 Observed increase in local cooling effect of deforestation at higher latitudes. *Nature*,
711 *479*(7373), 384–387. https://doi.org/10.1038/nature10588
712 Li, D., & Wang, L. (2019). Sensitivity of Surface Temperature to Land Use and Land Cover
713 Change-Induced Biophysical Changes: The Scale Issue. *Geophysical Research Letters*,
714 *46*(16), 9678–9689. https://doi.org/10.1029/2019GL084861
715 Mahmood, R., Pielke Sr., R. A., Hubbard, K. G., Niyogi, D., Dirmeyer, P. A., McAlpine, C., et
716 al. (2014). Land cover changes and their biogeophysical effects on climate. *International*
717 *Journal of Climatology*, *34*(4), 929–953. https://doi.org/10.1002/joc.3736
718 Manoli, G., Domec, J., Novick, K., Oishi, A. C., Noormets, A., Marani, M., & Katul, G. (2016).
719 Soil–plant–atmosphere conditions regulating convective cloud formation above
720 southeastern US pine plantations. *Global Change Biology*, *22*(6), 2238–2254.
721 https://doi.org/10.1111/gcb.13221

Mascioli, N. R., Previdi, M., Fiore, A. M., & Ting, M. (2017). Timing and seasonality of the United States' warming hole.' *Environmental Research Letters*, *12*(3), 034008. https://doi.org/10.1088/1748-9326/aa5ef4

Meehl, G. A., Arblaster, J. M., & Branstator, G. (2012). Mechanisms Contributing to the Warming Hole and the Consequent U.S. East–West Differential of Heat Extremes. *Journal of Climate*, *25*(18), 6394–6408. https://doi.org/10.1175/JCLI-D-11-00655.1

Metzger, S., Ayres, E., Durden, D., Florian, C., Lee, R., Lunch, C., et al. (2019). From NEON Field Sites to Data Portal: A Community Resource for Surface–Atmosphere Research Comes Online. *Bulletin of the American Meteorological Society*, *100*(11), 2305–2325. https://doi.org/10.1175/BAMS-D-17-0307.1

Mildrexler, D.J., Zhao, M. and Running, S.W., 2011. A global comparison between station air temperatures and MODIS land surface temperatures reveals the cooling role of forests. *Journal of Geophysical Research: Biogeosciences*, *116*(G3).

Monin, A. S., & Obukhov, A. M. (1954). Basic laws of turbulent mixing in the surface layer of the atmosphere. *Contrib. Geophys. Inst. Acad. Sci. USSR*, *151*(163), e187.

Mueller, N. D., Butler, E. E., McKinnon, K. A., Rhines, A., Tingley, M., Holbrook, N. M., & Huybers, P. (2016). Cooling of US Midwest summer temperature extremes from cropland intensification. *Nature Climate Change*, *6*(3), 317–322. https://doi.org/10.1038/nclimate2825

Nolan, C. J., Field, C. B., & Mach, K. J. (2021). Constraints and enablers for increasing carbon storage in the terrestrial biosphere. *Nature Reviews Earth & Environment*, *2*(6), 436–446. https://doi.org/10.1038/s43017-021-00166-8

Novick, K., & Katul, G. G. (2020). The Duality of Reforestation Impacts on Surface and Air Temperature. *Journal of Geophysical Research: Biogeosciences*, *125*(4). https://doi.org/10.1029/2019JG005543

Novick, K., Metzger, S., Anderegg, W. R. L., Barnes, M., Cala, D. S., Guan, K., et al. (2022a). Informing Nature-based Climate Solutions for the United States with the best-available science. *Global Change Biology*, *28*(12), gcb.16156. https://doi.org/10.1111/gcb.16156

Novick, K., Jo, I., D'Orangeville, L., Benson, M., Au, T. F., Barnes, M., et al. (2022b). The Drought Response of Eastern US Oaks in the Context of Their Declining Abundance. *BioScience*, *72*(4), 333–346. https://doi.org/10.1093/biosci/biab135

Novick, K., Biederman, J. A., Desai, A. R., Litvak, M. E., Moore, D. J., Scott, R. L., & Torn, M. S. (2018). The AmeriFlux network: A coalition of the willing. *Agricultural and Forest Meteorology*, *249*, 444–456. https://doi.org/10.1016/j.agrformet.2017.10.009

Pan, Y., Chen, J. M., Birdsey, R., McCullough, K., He, L., & Deng, F. (2012). NACP Forest Age Maps at 1-km Resolution for Canada (2004) and the U.S.A. (2006), 86.708785 MB. https://doi.org/10.3334/ORNLDAAC/1096

Pan, Z., Arritt, R. W., Takle, E. S., Gutowski, W. J., Anderson, C. J., & Segal, M. (2004). Altered hydrologic feedback in a warming climate introduces a "warming hole." *Geophysical Research Letters*, *31*(17). https://doi.org/10.1029/2004GL020528

Partridge, T. F., Winter, J. M., Osterberg, E. C., Hyndman, D. W., Kendall, A. D., & Magilligan, F. J. (2018). Spatially Distinct Seasonal Patterns and Forcings of the U.S. Warming Hole. *Geophysical Research Letters*, *45*(4), 2055–2063. https://doi.org/10.1002/2017GL076463

Pongratz, J., Reick, C. H., Raddatz, T., & Claussen, M. (2010). Biogeophysical versus biogeochemical climate response to historical anthropogenic land cover change: climate

effects of historical land cover change. *Geophysical Research Letters*, *37*(8). https://doi.org/10.1029/2010GL043010

Pongratz, J., Schwingshackl, C., Bultan, S., Obermeier, W., Havermann, F., & Guo, S. (2021). Land Use Effects on Climate: Current State, Recent Progress, and Emerging Topics. *Current Climate Change Reports*, *7*(4), 99–120. https://doi.org/10.1007/s40641-021-00178-y

R Core Team. (2020). R: A language and environment for statistical computing. Vienna, Austria: R Foundation for Statistical Computing. Retrieved from https://www.R-project.org/

Ramankutty, N., Heller, E., & Rhemtulla, J. (2010). Prevailing Myths About Agricultural Abandonment and Forest Regrowth in the United States. *Annals of the Association of American Geographers*, *100*(3), 502–512. https://doi.org/10.1080/00045601003788876

Rogers, J. C. (2013). The 20th century cooling trend over the southeastern United States. *Climate Dynamics*, *40*(1), 341–352. https://doi.org/10.1007/s00382-012-1437-6

Seddon, N., Chausson, A., Berry, P., Girardin, C. A. J., Smith, A., & Turner, B. (2020). Understanding the value and limits of nature-based solutions to climate change and other global challenges. *Philosophical Transactions of the Royal Society B: Biological Sciences*, *375*(1794), 20190120. https://doi.org/10.1098/rstb.2019.0120

Sohl, T. L., Sayler, K. L., Drummond, M. A., & Loveland, T. R. (2007). The FORE-SCE model: a practical approach for projecting land cover change using scenario-based modeling. *Journal of Land Use Science*, *2*(2), 103–126. https://doi.org/10.1080/17474230701218202

Spangler, K., Burchfield, E. K., & Schumacher, B. (2020). Past and Current Dynamics of U.S. Agricultural Land Use and Policy. *Frontiers in Sustainable Food Systems*, *4*, 98. https://doi.org/10.3389/fsufs.2020.00098

Stoy, P.C., Chu, H., Dahl, E., Cala, D.S., Shyeyster, V., Wiester, S., Desai, A.R., Novick, K.A. (2023, *preprint*). The global distribution of paired eddy covariance towers. bioRxiv 2023.03.03.530958; doi: https://doi.org/10.1101/2023.03.03.530958

Swann, A. L., Fung, I. Y., Levis, S., Bonan, G. B., & Doney, S. C. (2010). Changes in Arctic vegetation amplify high-latitude warming through the greenhouse effect. *Proceedings of the National Academy of Sciences*, *107*(4), 1295–1300. https://doi.org/10.1073/pnas.0913846107

Swann, A. L. S., Fung, I. Y., & Chiang, J. C. H. (2012). Mid-latitude afforestation shifts general circulation and tropical precipitation. *Proceedings of the National Academy of Sciences*, *109*(3), 712–716. https://doi.org/10.1073/pnas.1116706108

Swann, A. L. S., Laguë, M. M., Garcia, E. S., Field, J. P., Breshears, D. D., Moore, D. J. P., et al. (2018). Continental-scale consequences of tree die-offs in North America: identifying where forest loss matters most. *Environmental Research Letters*, *13*(5), 055014. https://doi.org/10.1088/1748-9326/aaba0f

Thornton, P.E., Thornton, M.M., Mayer, B.W., Wei, Y., Devarakonda, R., Vose, R.S., & Cook, R.B. (2016). Daymet: Daily Surface Weather Data on a 1-km Grid for North America, Version 3 (Version 3.4) [NetCDF], 0 MB. https://doi.org/10.3334/ORNLDAAC/1328

Tosca, M. G., Campbell, J., Garay, M., Lolli, S., Seidel, F. C., Marquis, J., & Kalashnikova, O. (2017). Attributing Accelerated Summertime Warming in the Southeast United States to Recent Reductions in Aerosol Burden: Indications from Vertically-Resolved Observations. *Remote Sensing*, *9*(7), 674. https://doi.org/10.3390/rs9070674

812 Verbesselt, J., Hyndman, R., Zeileis, A., & Culvenor, D. (2010). Phenological change detection
813 while accounting for abrupt and gradual trends in satellite image time series. *Remote*
814 *Sensing of Environment*, *114*(12), 2970–2980. https://doi.org/10.1016/j.rse.2010.08.003
815 Verbesselt, J., Zeileis, A., & Herold, M. (2012). Near real-time disturbance detection using
816 satellite image time series. *Remote Sensing of Environment*, *123*, 98–108.
817 https://doi.org/10.1016/j.rse.2012.02.022
818 Wan, Z., Hook, S., & Hulley, G. (2015). MYD11A1 MODIS/Aqua Land Surface
819 Temperature/Emissivity Daily L3 Global 1km SIN Grid V006 [Data set]. NASA
820 EOSDIS Land Processes DAAC. https://doi.org/10.5067/MODIS/MYD11A1.006
821 Wear, D. N., & Greis, J. G. (2012). The Southern Forest Futures Project: summary report. *Gen.*
822 *Tech. Rep. SRS-GTR-168. Asheville, NC: USDA-Forest Service, Southern Research*
823 *Station. 54 p.*, *168*, 1–54.
824 Williams, C. A., Gu, H., & Jiao, T. (2021). Climate impacts of U.S. forest loss span net warming
825 to net cooling. *Science Advances*, *7*(7), eaax8859. https://doi.org/10.1126/sciadv.aax8859
826 Willmott, C. J., & Matsuura, K. (1995). Smart Interpolation of Annually Averaged Air
827 Temperature in the United States. *Journal of Applied Meteorology*, *34*(12), 2577–2586.
828 https://doi.org/10.1175/1520-0450(1995)034<2577:SIOAAA>2.0.CO;2
829 Willmott, C. J., & Matsuura, K. (n.d.). Terrestrial Air Temperature and Precipitation: Monthly
830 and Annual Time Series (V4.01; 1900-2014). Retrieved August 6, 2019, from
831 http://climate.geog.udel.edu/~climate/html_pages/README.ghcn_ts2.html
832 Winckler, J., Reick, C. H., Luyssaert, S., Cescatti, A., Stoy, P. C., Lejeune, Q., et al. (2019).
833 Different response of surface temperature and air temperature to deforestation in climate
834 models. *Earth System Dynamics*, *10*(3), 473–484. https://doi.org/10.5194/esd-10-473-
835 2019
836 Windisch, M. G., Davin, E. L., & Seneviratne, S. I. (2021). Prioritizing forestation based on
837 biogeochemical and local biogeophysical impacts. *Nature Climate Change*, *11*(10), 867–
838 871. https://doi.org/10.1038/s41558-021-01161-z
839 Wutzler, T., Lucas-Moffat, A., Migliavacca, M., Knauer, J., Sickel, K., Šigut, L., et al. (2018).
840 Basic and extensible post-processing of eddy covariance flux data with REddyProc.
841 *Biogeosciences*, *15*(16), 5015–5030. https://doi.org/10.5194/bg-15-5015-2018
842 Zhang, Q., Barnes, M., Benson, M., Burakowski, E., Oishi, A. C., Ouimette, A., et al. (2020).
843 Reforestation and surface cooling in temperate zones: Mechanisms and implications.
844 *Global Change Biology*, *26*(6), 3384–3401. https://doi.org/10.1111/gcb.15069
845